LA-UR-21-28606
Approved for public release; distribution is unlimited.

Title: 2021 Summer SPE project

Author(s): Lee, Yu-Hsuan
Larmat, Carene
Lei, Zhou

Intended for: Report

Issued: 2021-08-30

2021 Summer SPE Project

20th August 2021

Yu-Hsuan Lee[1], Carene Larmat[1], Zhou Lei[1]; [1] EES-17, Los Alamos National Laboratory

OVERVIEW

SPE is a project in order to develop new, more physics-based, seismic models of explosions (see Nelson et al. 2013). One key component of this effort is numerical modeling enabled by modern state-of-art code/software. Accurate modeling of the shape and amplitude of seismic waves from their generation to their propagation to remote monitoring seismic stations is important to our ability to determine the origin and strength of the source from remote recording.

In this project, the modeling is performed by coupling two codes HOSS and SPECFEM3D. HOSS models the dynamic nonlinear processes happening near the explosion. SPECFEM3D computes the propagation of seismic waves as they travel through 3D complex Earth models. SPECFEM3D was modified in order to be driven by a set of time-series calculated by HOSS in lieu of a seismic source. The goal of this summer project is the investigation of several questions pertinent to the establishment of a full end-to-end modeling capability from the high-rate strain regime area to remote distances where seismic station record seismic waves generated by explosions. The investigated questions are:

(1) How to perform proper filtering? Direct-solution modeling only sustains a limited range of frequency depending on the grid size. As we go from one modeling domain to the other via coupling, the mesh size is getting coarser to allow modeling at large scale but also to account for the fact that high-frequency waves do not physically travel to large distances. So filtering of the time-series generated by the near-field hydrodynamic modeling is a current practice often employed but its effects on the modeled waveforms has to be investigated.
(2) Quantitative assessment of the efficiency of attenuation to remove high-frequency content of the wavefield. This assessment will allow to create meshes with a grid size appropriate to the actual physics of wave propagation for a given explosion.
(3) Checking that the coupling process and the two codes respect the cylindrical symmetry that is expected in the case of a pure explosion in a half-space.
(4) The effect of the state-of-stress in the near-source area on the modeled seismic waveforms.

These questions will be investigated through the modeling of SPE-4P, the fourth explosion of this series because it was designed to have little interaction with the geologic surrounding and the free surface of the Earth so that it is the most explosion-like experiment, with the most symmetries to be verified.

The work was performed during a summer internship of 10 weeks, during which Yu-Hsuan Lee has learnt

MODELING

SPECFEM3D MODELING.

Fig.1 and table 1 show the geometry and parameters of the SPECFEM3D model. The red point in fig.1 represents the location of the explosion source. The model used for the coupling with HOSS is divided into three layers with different vertical size for the element of the SPECFEM3D grid, which will be explained later; but all layers have the same material parameters. Except for the top free surface, all other boundaries have Stacey absorbing boundary conditions to simulate a semi-infinite medium. However, reflection sometimes can still be generated with the boundary condition due to numerical error, so a deep enough depth of model is needed. The first tried model depth is 1007.2 m and reflection is observed. After increasing it to 4007.2 m, parasite reflections didn't appear as much in the monitored waveforms. The domain decomposition used for the parallelization of SPECFEM3D is based on the x-y coordinate. In our modeling, each processor handles 16*16*200=51200 elements.

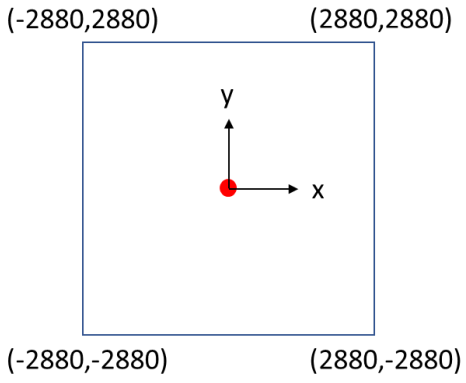

(a)

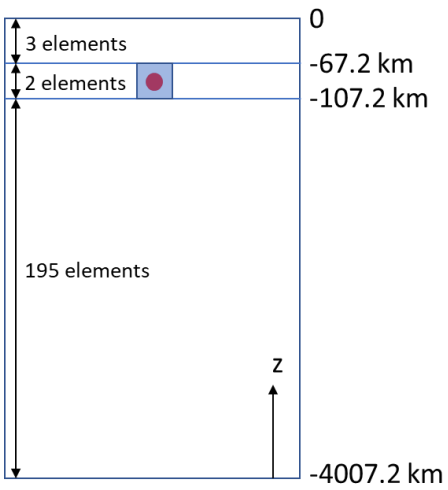

(b)

Figure 1: Model Geometry

Elements	288*288*50
Processors	18*18
Materials	
Density (kg/m3)	2680
P-wave velocity (m/s)	4727
S-wave velocity (m/s)	2613

Table 1: Model Parameters

NEAR-FIELD MODELING.

The Hybrid Optimization Software Suite, HOSS is the code we use to generate the high-strain-rate regime near the explosion. The coupling to SPECFEM3D is performed by providing time series generated by HOSS as displacement boundary condition to the SPECFEM3D code. For the model shown in fig.1, 600 time series are generated for a coupling box constituted of 600 points, with a time step of 3e-4 second and total time of 6 seconds. The coupling box is a cube shown as the blue box in fig.1, with size of 20m, and the center corresponds to the SPE-4P explosion source location. If the grid of SPECFEM3D is changed, both

the coupling box and the time-series computed by HOSS have to be changed to correspond to the new spatial and time sampling.

HOSS calculations were performed with the explosion happening in different state-of-stress of the column of rock surrounding the explosion. Explosions in real Earth don't happen in a free space but in a confined environment within the subsurface of the Earth where they are affected to an in-situ state-of-stress. The first source of this stress is the hydrostatic pressure created by the weight of the column of rock above the explosion. We are trying to quantify this effect by comparing the result when HOSS calculations are done in a hydrostatic state-of-stress versus when done with no state-of-stress. We also processed the time-series differently. The different cases and the naming convention are given in Table 2.

Near-field case #	Stress state in the near field	Source symmetry	Time-series Processing
1-fil	No stress state	spherical	Filtered 80Hz - apodization
1-fillp	No stress state	spherical	Filtered 80Hz two pass filter - apodization
1-nofil	No stress state	spherical	No filtering - apodization
2-fil	hydrostatic	cylindrical	Filtered 80Hz - apodization
2-fillp	hydrostatic	cylindrical	Filtered 80Hz two pass filter - apodization
2-nofil	hydrostatic	cylindrical	No filtering - apodization

Table 2: Different near-field scenario to run. Each scenario corresponds to a different state of stress that the near-field is subjected to and processing of the time-series. The original goal of this project is for you to run only two state-of-stress. There are two additional ones indicated that may be used if there is time and resources.

Results

Filter effect of time series processing

Fig.2 shows the velocity waveforms in the radial, tangential and vertical direction at a distance of 0.9km from the explosion location, with the 1-nofil, 1-fil, 2-nofil, 2-fil cases presented in table 2. In (a) and (d) are plotted the raw result of “fil” case and of “nofil” case, the later being filtered up to 80Hz with the one-pass scipy filter “lfilter”. In (b) and (e) are plotted the same time-series but both post-processed with a four-pole two-pass filter from seismic sac. In (c) and (f) are plotted the time-series post-processed with the same filter, but filtered to a frequency band of 2-8 Hz to observe potential surface waves. 80Hz was chosen to be the corner frequency of the filtering because the 20m elements of the SPECFEM3D mesh only sustain wave propagation up to 93Hz. With no filter, the waveform contains numerical noise that masks any physical and resolved signal. Results of fig.2 show a time-shift between no-fil case and fil case in (b), (c), (e), (f), but not in (a) and (d) case. Since the time series of “fil” case is filtered with the one -pass filter, this result suggests that it introduces a time-shift. As there’s no time-shift in (a) and (d) while using one-pass filter for post-processing, it is surmised that the time-shift in (b), (c), (e), (f) is caused by the pre-coupling filtering of time series, instead of generated in the SPECFEM3D simulation. To verify, 1-fillp and 2-fillp time series are generated and filtered with the four-pole two-pass filter, corresponding to the cases fillp of table 2.

Fig.3 shows the result at the same location with “nofil” and “fillp” case, post-processed with the four-pole two-pass filter. Most of the results show no time-shift, but with amplitude difference. And for the no-stress-state case, the surface wave (fig.3(b)) is showing a time shift between nofil and fillp case at the surface wave frequencies but the signal is very weak.

Combining the observation of fig.2 and 3, it shows that filtering before or after the coupling is equivalent through the case of the one pass-filter which shows identical waveform produced; but it is known that the usage of one-pass filter introduce time-shift . The no-match in the case of the two-pass filter may be due to the difference of pre-processing that the two time-series are affected to; which is apodization and zero-tapering for the pre-coupling filtering and none for the post-coupling filtering. The filtering and processing effects need more clarification.

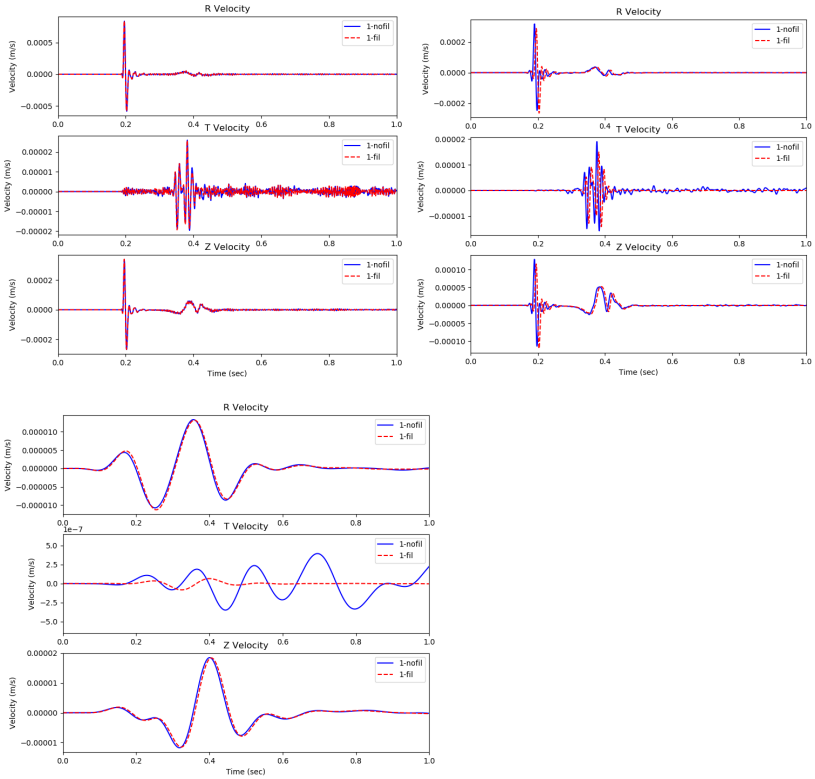
R Velocity
T Velocity
Z Velocity
1-nofil
1-fil
Velocity (m/s)
Time (sec)

(a) (b) (c)

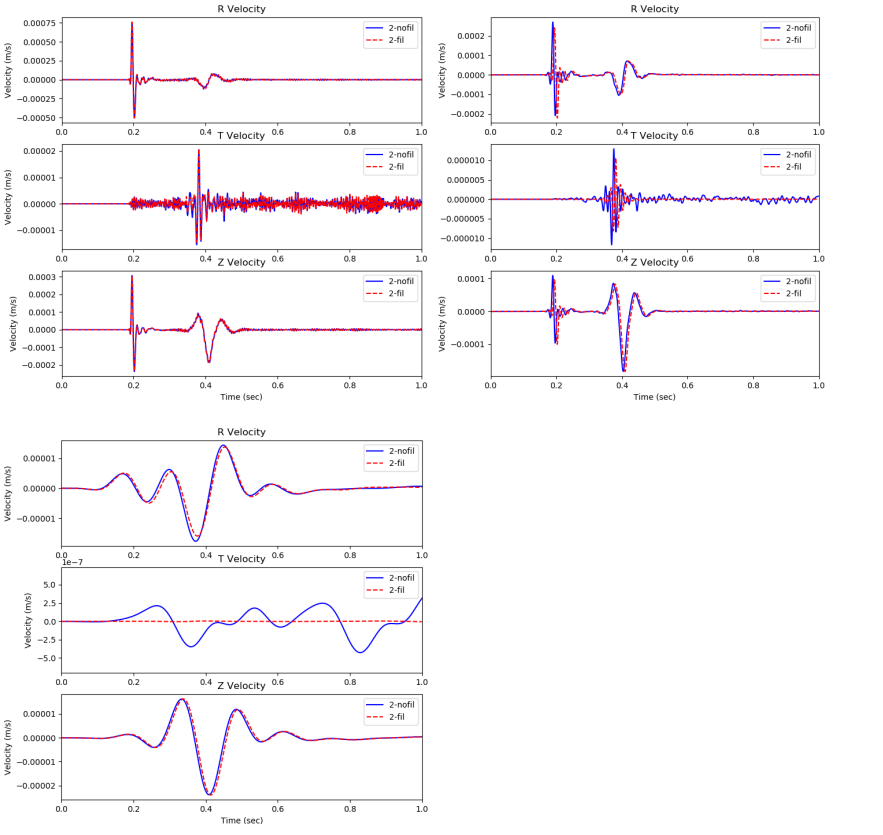
R Velocity
T Velocity
Z Velocity
2-nofil
2-fil
Velocity (m/s)
Time (sec)

(d) (e) (f)

Figure 2: Velocity waveforms at a distance of 0.9 km. (a)-(c) are plotted with no stress state case, (d)-(f) are plotted with the hydrostatic case. (a) and (d) are raw data with the nofil case having post-processing one-dimensional filtering with 80 Hz. (b) and (e) are 80 Hz filtered with the two-pass filter, and same for (c) and (f) with 2-8 Hz.

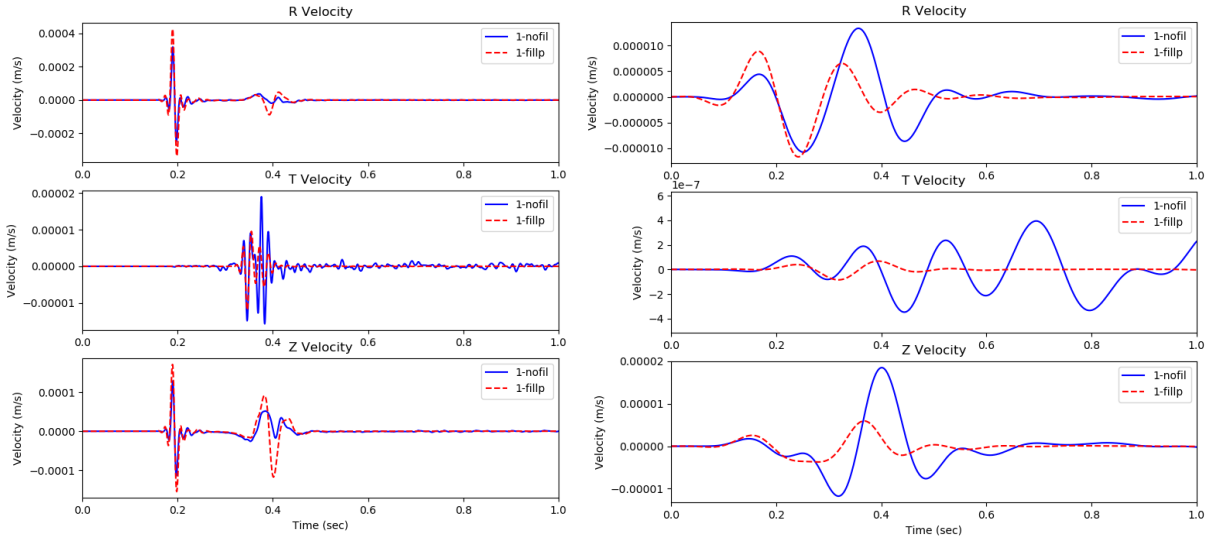

(a) (b)

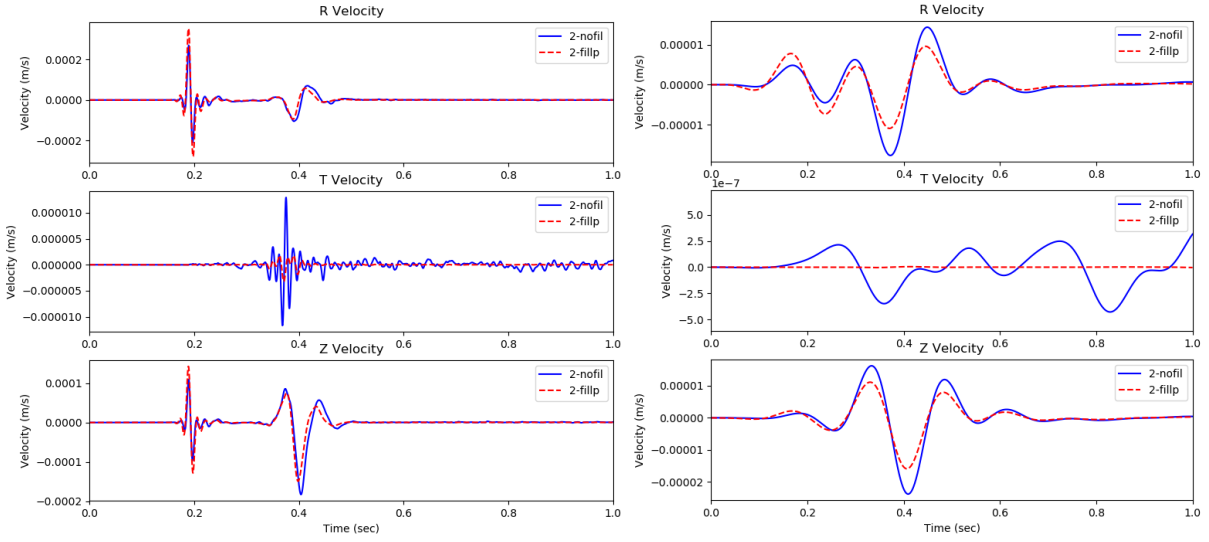

(c) (d)

Figure 3: Velocity waveforms at a distance of 0.9 km. (a) and (b) are plotted with no stress state case, (c)-(d) are plotted with the hydrostatic case. (a) and (c) are 85 Hz filtered, (b) and (d) are 2-8 Hz filtered.

Attenuation study

To study the effect of attenuation, the run1-fil case is run with attenuation that is defined through the seismic "Quality factor" in SPECFEM3D. The quality factors used in the code are Qκ and Qμ instead of Qp and Qs which are usually used. The relationship between these different quality factors are given by Anderson & Hart (1978) :

$$L = 4.0/3.0 * (vs/vp)^2$$

$$Q_{mu} = Q_s$$

$$Q_{kappa} = (1.0 - L) * Q_p * Q_s/(Q_s - LQ_p)$$

In the following result, the parameters used are Qκ=1926.72 and Qμ=130, which are generated automatically by SPECFEM3D. The result of comparing run1-fil with and without attenuation are shown in fig.4.

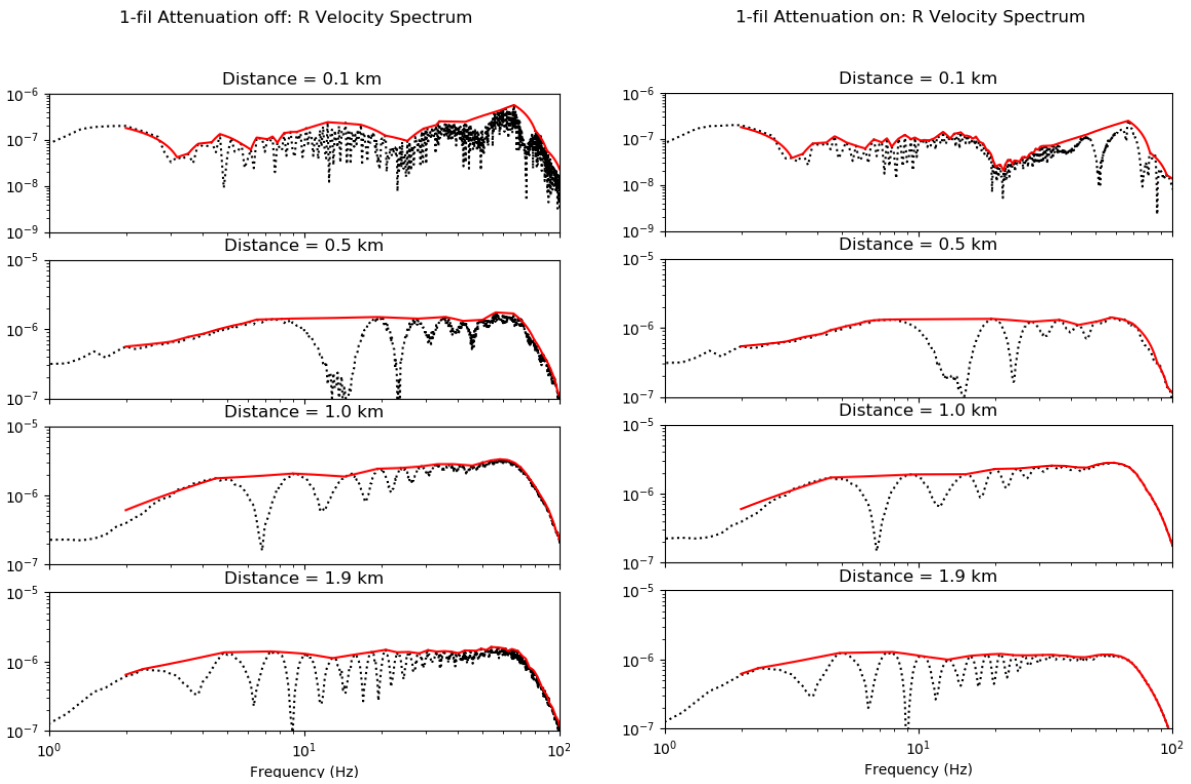

(a) (b)

Figure 4: Spectrum of no stress state pre-filtered case (a) without attenuation (b) with attenuation

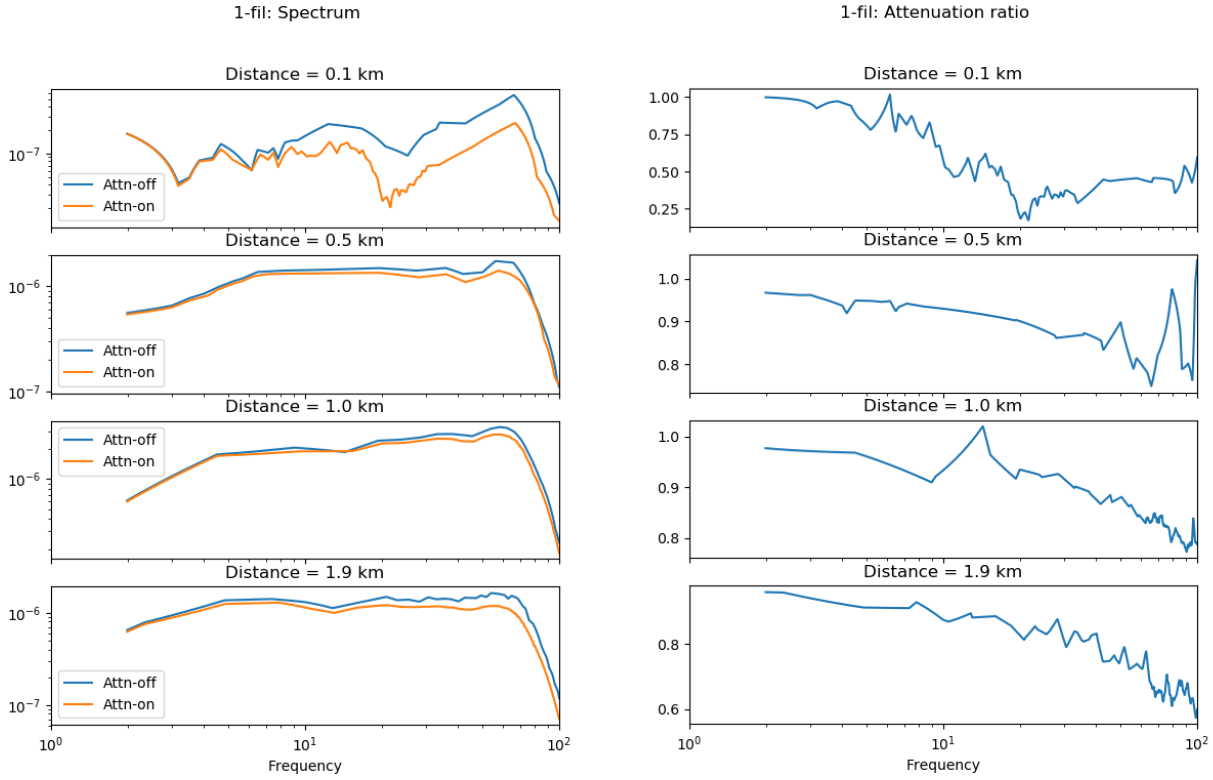

(a) (b)

Figure 5: (a) Peak curves of spectrum (b) ratio of the two peak curves

Fig.4 shows the absolute spectrum of the two cases. Since the time step is quite small, the spectrum generated directly by Fast Fourier Transformation has a high density of frequency data, which caused a lot peaks on the spectrum. We use an algorithm to extract the peak of the spectra for easier comparison. The “peak curve” is plotted as the red curve in fig.4. Fig.5 shows the comparison of two peak curves and a plot of their ratio. We can see there’s a strong effect of attenuation on the amplitude of the spectra around 0.1 km, and increasing attenuation from 0.5 km to 1.9 km. Also, we can see that high frequency waves are affected by higher attenuation than low frequency waves.

Verification of pure SPECFEM3D and Coupling results

When modeling the explosion with SPECFEM3D, the simulation is entirely elastic, while the physics s modeled by HOSS includes inelasticity and shock wave effects. In the following, we compare the displacement on several points of the coupling box. Fig.6 shows the displacement at four corners of the coupling box, as the source of the seismic simulation. First of all, it shows that the pure SPECFEM3D result is not symmetric, since it has a closer result with the waveform modeled by HOSSe for x=-20, y=-20, and more different for x=20 and y =20. Also, it shows that the HOSS modeled waveform has the peak earlier than the pure elastic case, as well as a higher amplitude.

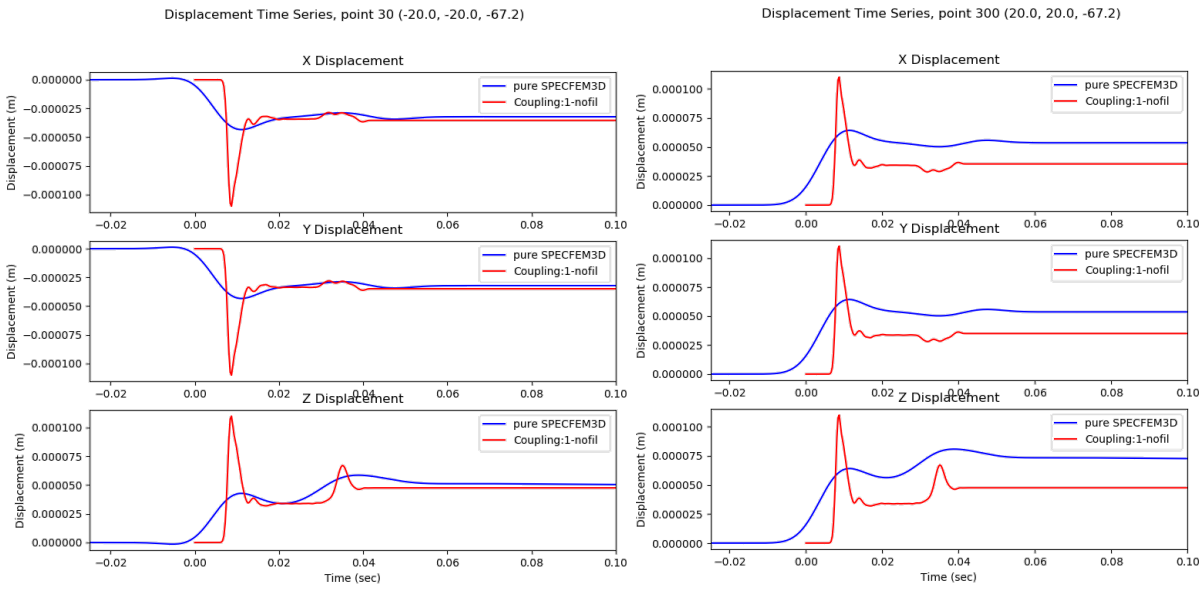

(a) (b)

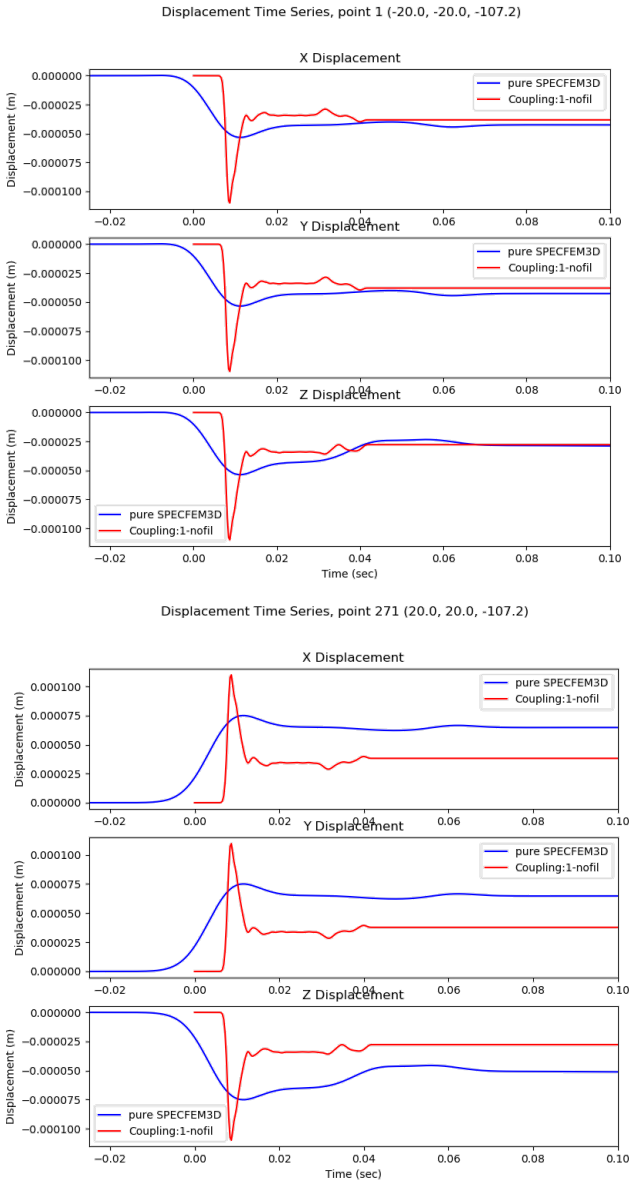

(c) (d)

Figure 6: Displacement time series of four corners of coupling box

Fig. 7 shows the velocity waveforms at a distance of 0.9 km comparing the pure elastic case with the case run 1 modeled by HOSS. For high frequency (fig. 7(a)), the two cases peak at the same time for the first wave. For the second wave, the HOSS coupled case peaks later. Also, it can be observed that the HOSS coupled case has a higher frequency content than the elastic case. For the surface waves frequency band (fig.7(b)), the HOSS coupled case peaks later than the elastic case, but the two curves overlap after 0.6 second in both the R and Z directions. They looked different in the transverse (T) direction, but this component is not expected to contain any signal and indeed displays a small amplitude and can be considered as noise.

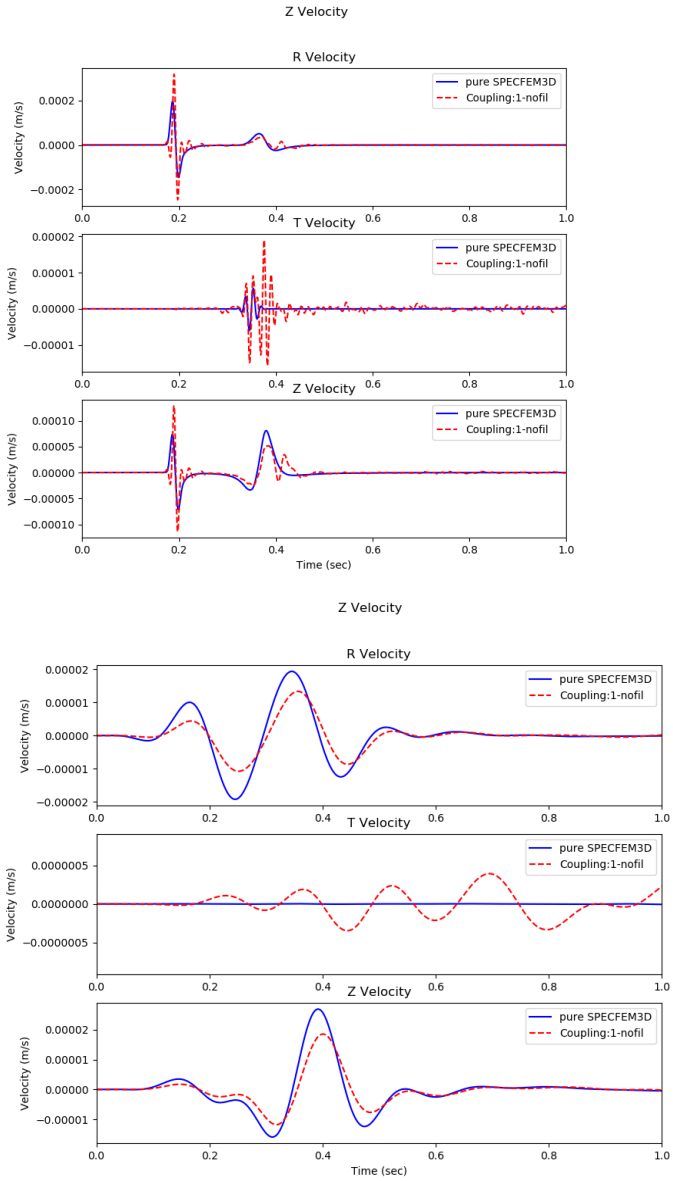

(a) (b)

Figure 7: Velocity waveforms at a distance of 0.9 km. (a) 85 Hz filtered (b) 2-8 Hz filtered.

In order to assimilate the results for more data, the max difference between the waveforms modeled in the purely elastic case and the HOSS coupled case for 720 surface stations results are plotted in fig. 8. If there is any variance in the results at a given distance, it means the results are different at different azimuth. The scattered results in the transverse direction are expected to be noise because of the cylindrical symmetry of the problem and thus can be ignored. For high frequency waves, it shows that there are differences in the radial (R) component at 0.25 km, and at 0.75 km for the vertical (Z) direction. Fig. 9 plotted the time at wmaximum difference happened time, which can be used to check if the difference is from noise, and which wave is having the

maximum difference. By comparing fig.8(a), (b) and fig.9(a), we can know that at the distance of 0.25 km there aretwo waves mixed together which are at the origin of the observed differences. For distances larger than 0.25 km the two waves got separated. In the radial (R) direction, at 0.5 km the maximum difference occurs with the second wave, then with the first wave, and at 0.75 km for the Z direction. For low frequency band (fig. 9 b), we can also know that in 0.25 km waves are mixed together, but the dominating wave for maximum difference seems to keep changing with the distance. Also, it shows that although the source displacement of the two cases are asymmetric, the differences for longer distance seems no difference for different azimuths. The reason might be the size of the coupling box. Since the box is quite small, waves are complicated at that distance, which will cause different displacement in different azimuthal directions.

To check the above behavior, distance-time plots are plotted in Figure 10 for one azimuth direction. For high frequency content, it is obvious that the first wave is P-wave, and the second wave would be S-wave or Rayleigh wave. For low frequency content, we can also see different waves. But due to the frequency, they don't look very separated during the simulation time.

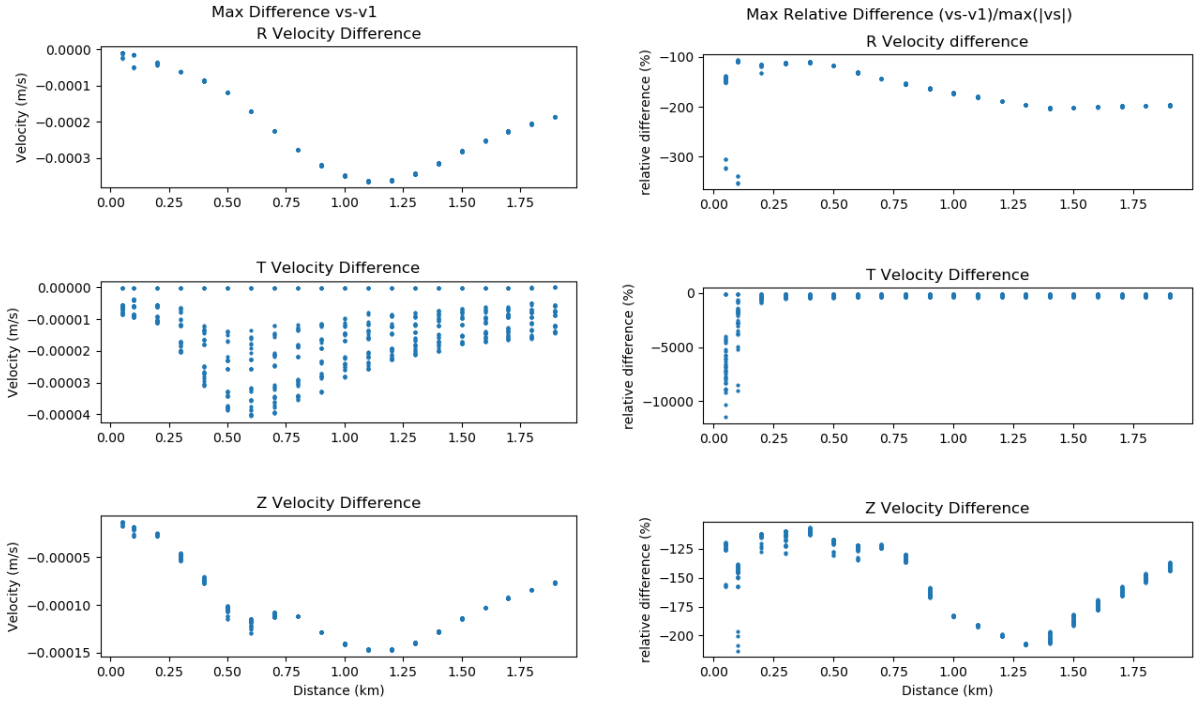

(a) (b)

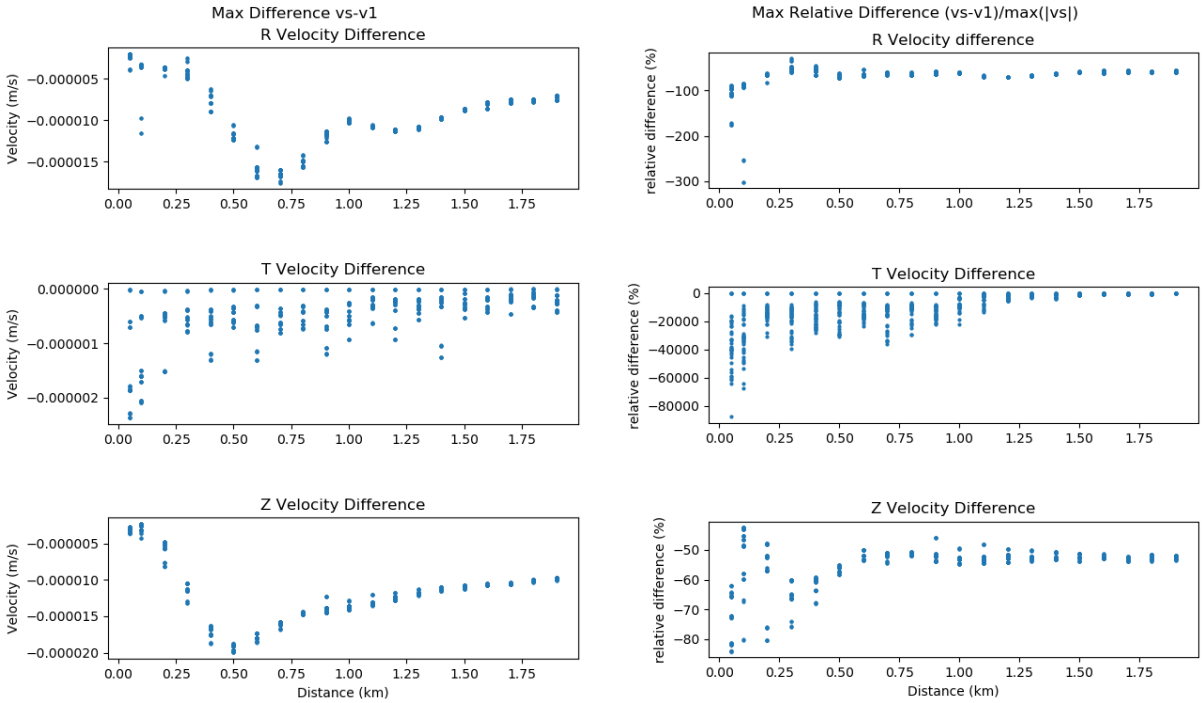

(c) (d)

Figure 8: Maximum velocity differences with distance, (a) and (c) are differences, (b) and (d) are relative differences. (a) and (b) are 85 Hz filtered, (c) and (d) are 2-8 Hz filtered.

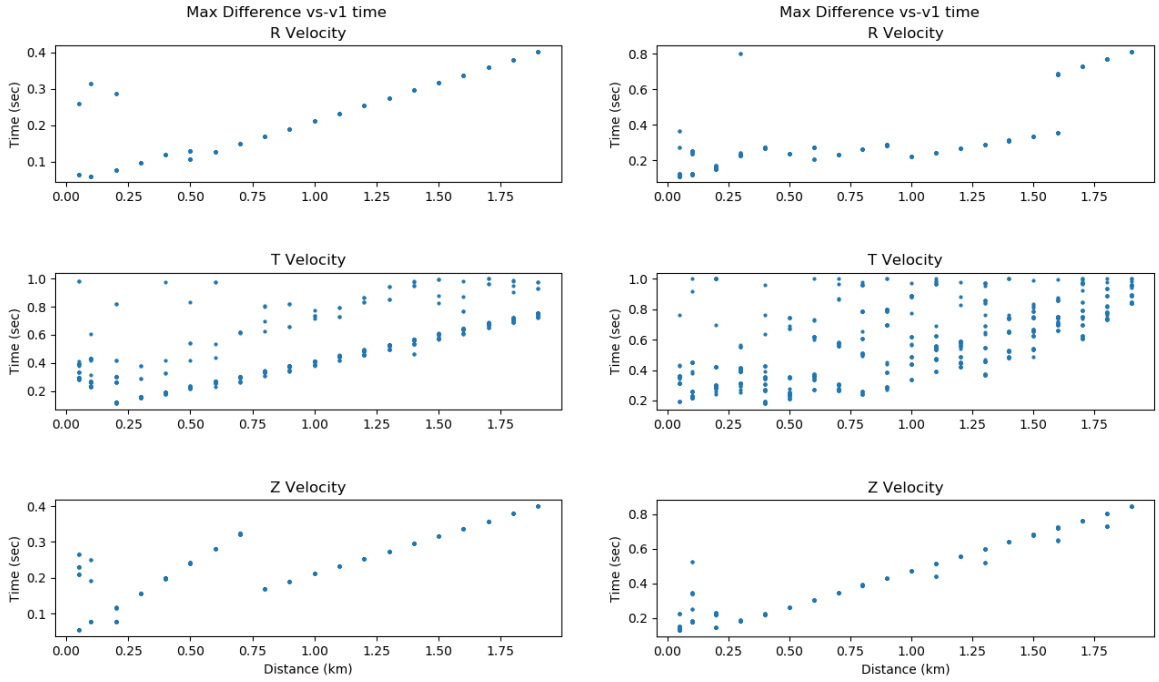

(a) (b)

Figure 9: Time at which the maximum velocity difference occurs (a) 85 Hz filtered (b) 2-8 Hz filtered.

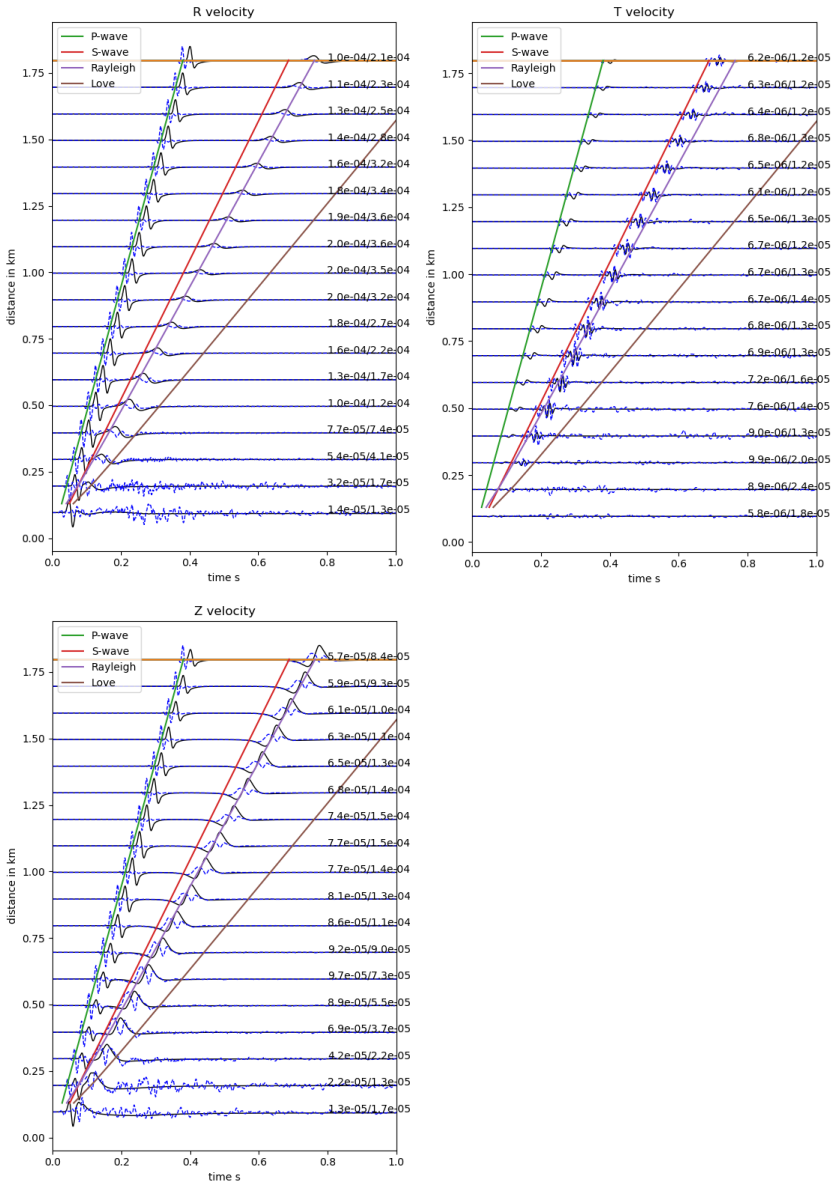

(a) (b) (c)

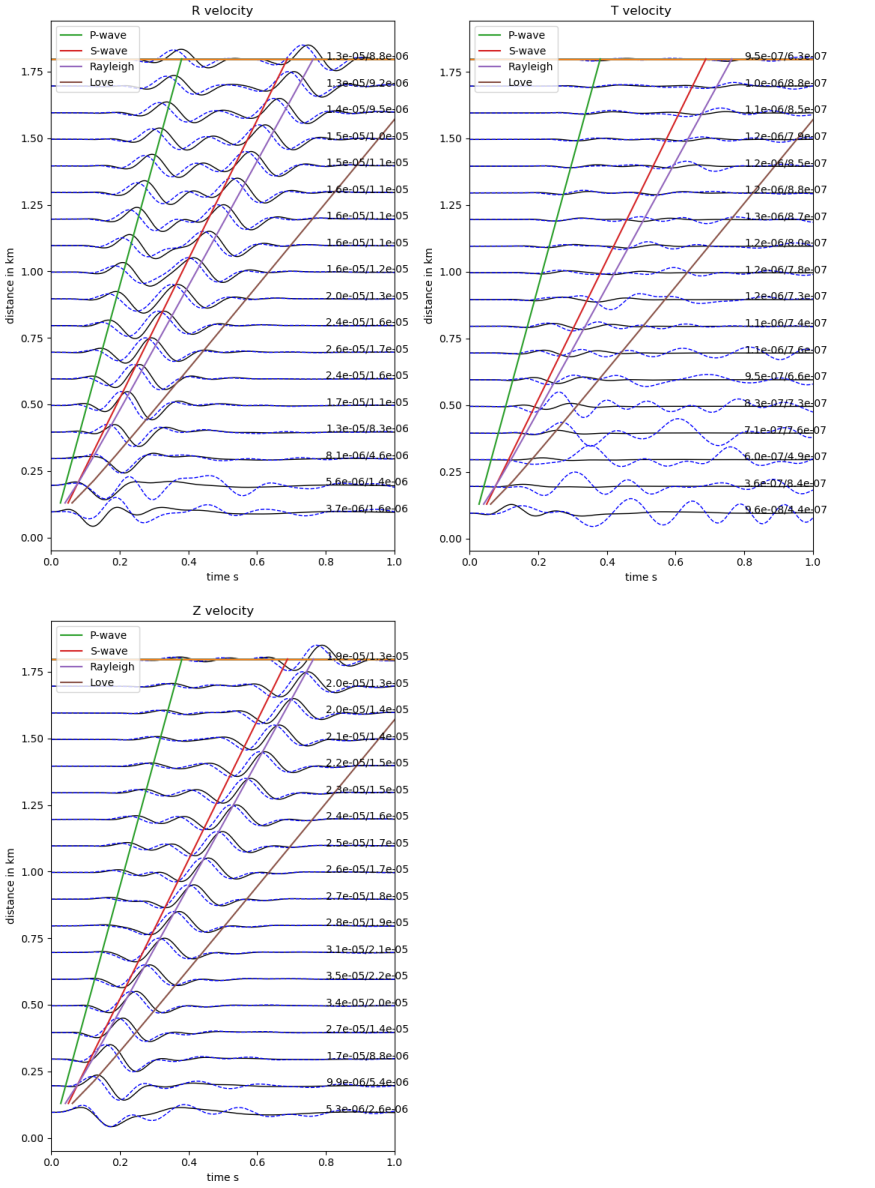

(d) (e) (f)

Figure 10: Distance-time plot of velocity. (a)-(c) 85 Hz filtered (d)-(f) 2-8 Hz filtered.

Comparison of stress state

Fig. 11 shows the displacement time series of the no-stress-state case and hydrostatic case for the source of SPECFEM3D. The no-stress-state case peaks with a higher amplitude than the hydrostatic case. The horizontal results are a little bit symmetric. For the vertical direction, the two cases look quite different. At top of the coupling box, the displacement of no-stress-state case increased after the first peak, while hydrostatic case decreased; at bottom of the coupling box, the displacement of no-stress-state case decreased after the first peak, while the hydrostatic

case increased and had higher value than no-stress-state case. The horizontal result might be different for the same reason above-mentioned, due to the complicated wave in short distance. The difference in vertical direction should be because of the stress state.

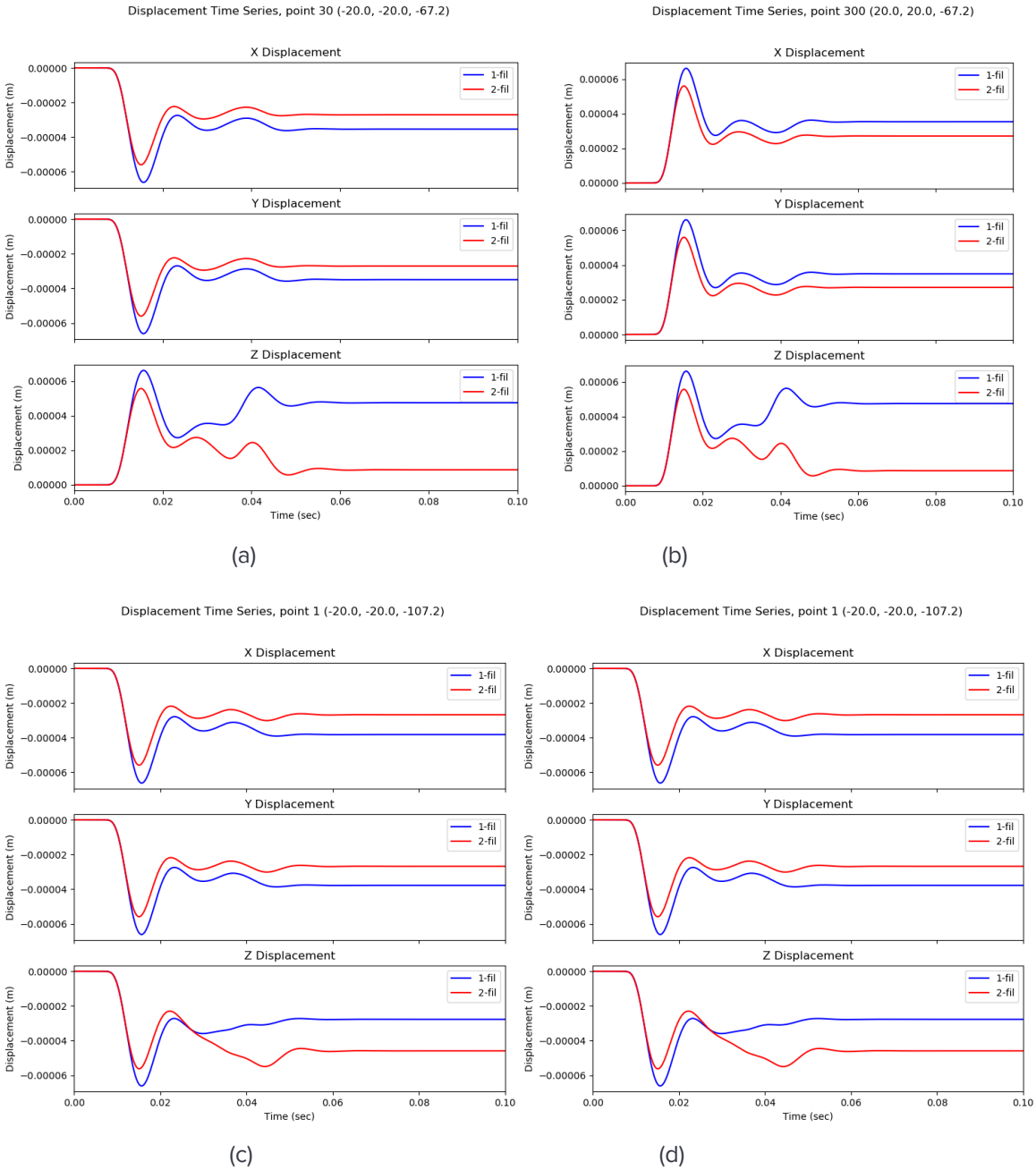

Figure 11: Displacement time series of four corners of coupling box

Figure 12 shows the result at a distance of 0.9 km. For high frequency, the two cases have similar wave shape for the first wave, with 1-fil has higher amplitude; The case run2-fil has higher amplitude and lower frequency for the second wave. This might have a relationship with the increasing value in fig.10(c) and (d) Z direction. For low frequency, the two cases have quite

different results. Not only time-shift, but also the wave shape. It might need some verification for the low frequency data generation, but since the increase of the case run2-fil in fig.11(c) and (d) looks like a very low frequency wave, it might give effection to the frequency wave. Fig.13 shows multiple maximum differences of the two cases. The scattered result in T direction is considered as noise. For high frequency band, there are no big differences for different azimuths. But the behavior of the difference changes quite differently around 0.6 km. For the low frequency band, there are more differences for different azimuths. By comparing the maximum difference happened time (fig.14) and the distance-time plot (fig.15), we can infer that for high frequency case, the difference change at 0.6 km is due to separation of the two waves, and most of the max difference corresponds to the second wave; for the low frequency band, though the maximum difference changes with different azimuths, most of them happen at the same time, which is the same wave. Again in fig.15, it shows that the first wave should be P-wave and the second wave might be S-wave or Rayleigh wave.

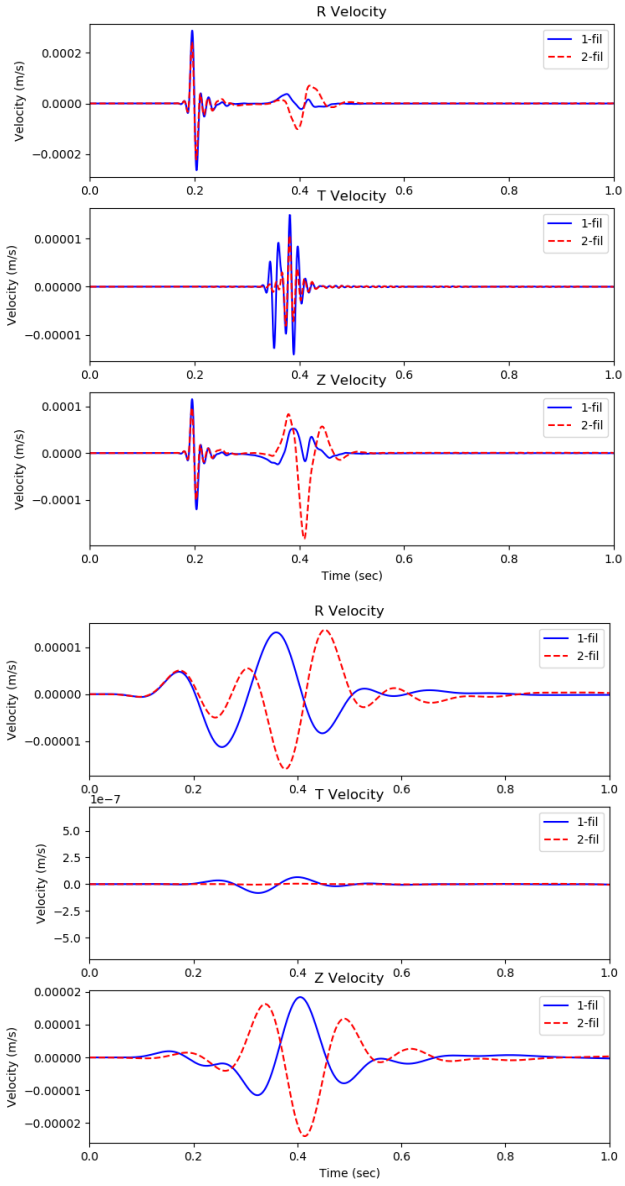

(a) (b)

Figure 12: Velocity results at a distance of 0.9 km. (a) 85 Hz filtered (b) 2-8 Hz filtered.

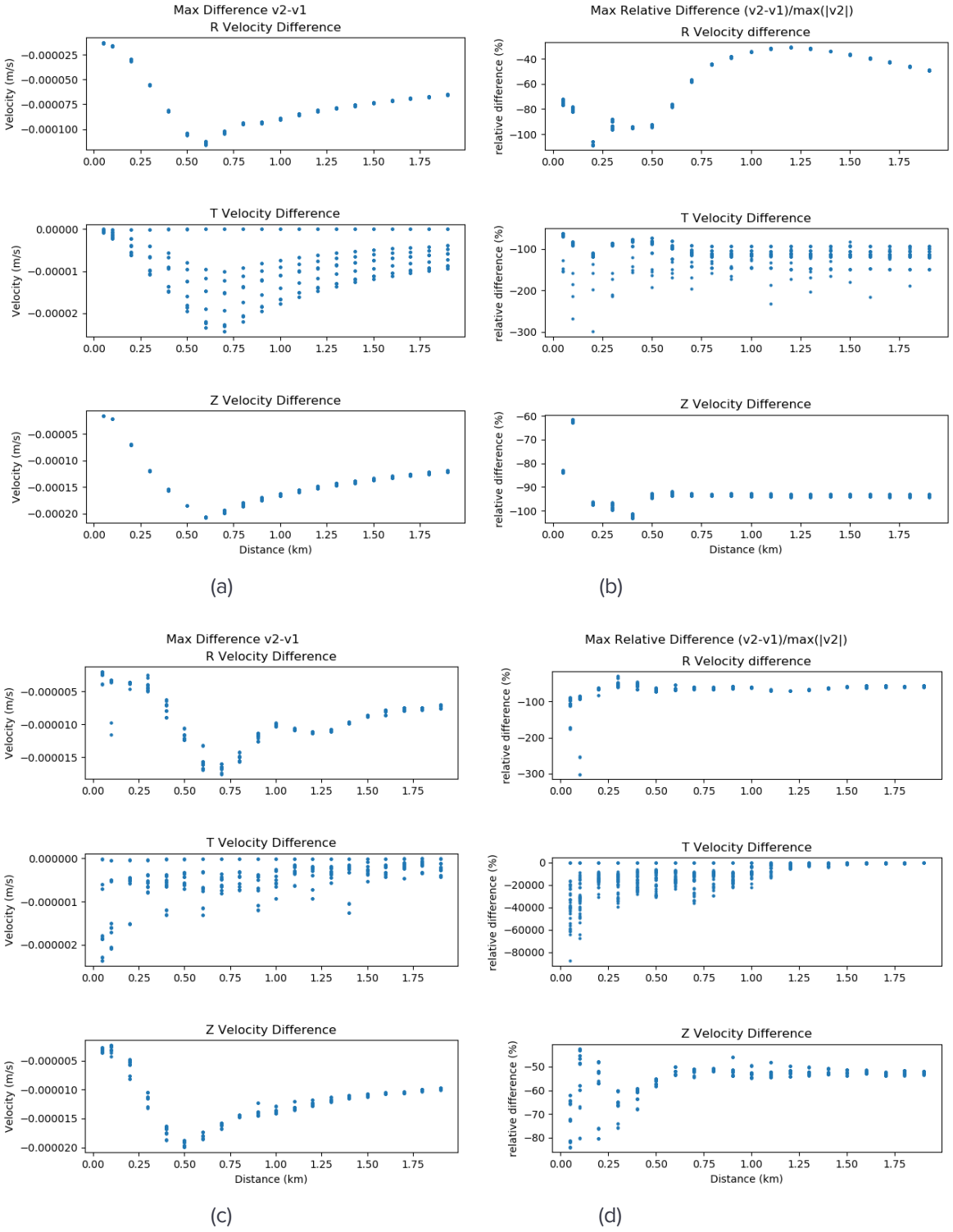

Figure 13: Maximum velocity differences with distance, (a) and (c) are difference, (b) and (d) are relative difference. (a) and (b) are 85 Hz filtered, (c) and (d) are 2-8 Hz filtered.

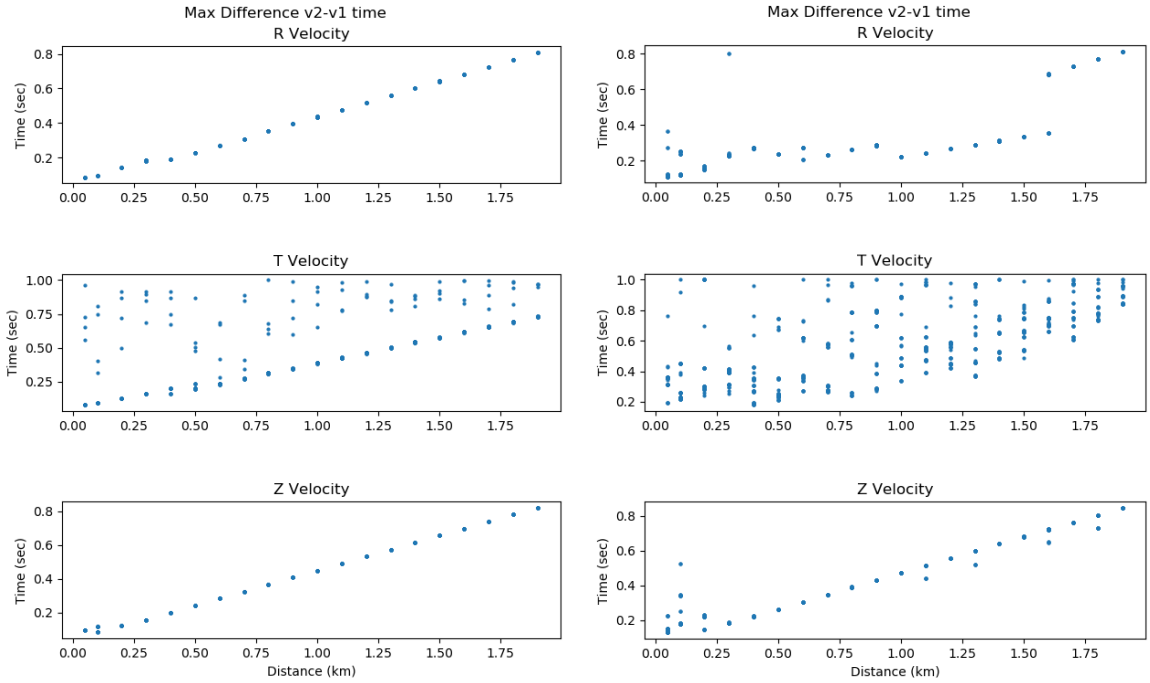

Figure 14: Maximum velocity difference happened time. (a) 85 Hz filtered (b) 2-8 Hz filtered.

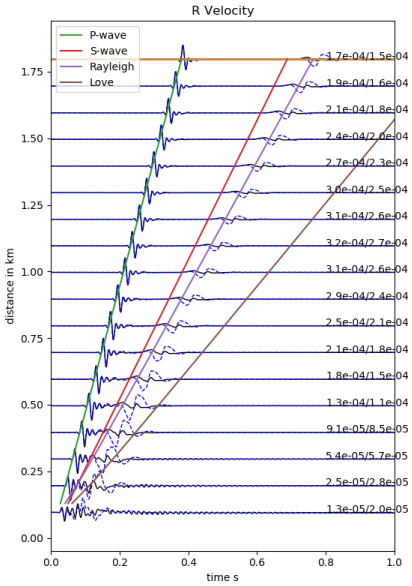
R Velocity
P-wave
S-wave
Rayleigh
Love
distance in km
time s
1.7e-04/1.5e-04
1.9e-04/1.6e-04
2.1e-04/1.8e-04
2.4e-04/2.0e-04
2.7e-04/2.3e-04
3.0e-04/2.5e-04
3.1e-04/2.6e-04
3.2e-04/2.7e-04
3.1e-04/2.6e-04
2.9e-04/2.4e-04
2.5e-04/2.1e-04
2.1e-04/1.8e-04
1.8e-04/1.5e-04
1.3e-04/1.1e-04
9.1e-05/8.5e-05
5.4e-05/5.7e-05
2.5e-05/2.8e-05
1.3e-05/2.0e-05

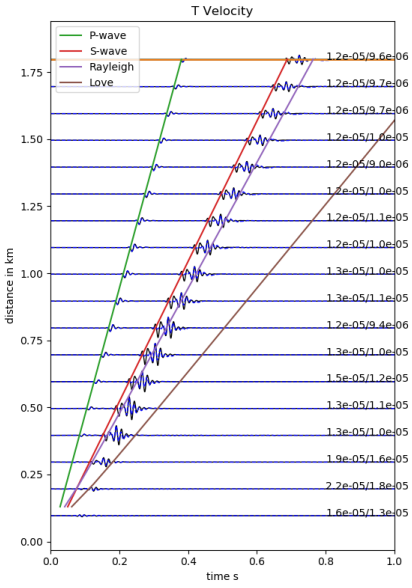
T Velocity
P-wave
S-wave
Rayleigh
Love
distance in km
time s
1.2e-05/9.6e-06
1.2e-05/9.7e-06
1.2e-05/9.7e-06
1.2e-05/1.0e-05
1.2e-05/9.0e-06
1.2e-05/1.0e-05
1.2e-05/1.1e-05
1.2e-05/1.0e-05
1.3e-05/1.0e-05
1.3e-05/1.1e-05
1.2e-05/9.4e-06
1.3e-05/1.0e-05
1.5e-05/1.2e-05
1.3e-05/1.1e-05
1.3e-05/1.0e-05
1.9e-05/1.6e-05
2.2e-05/1.8e-05
1.6e-05/1.3e-05

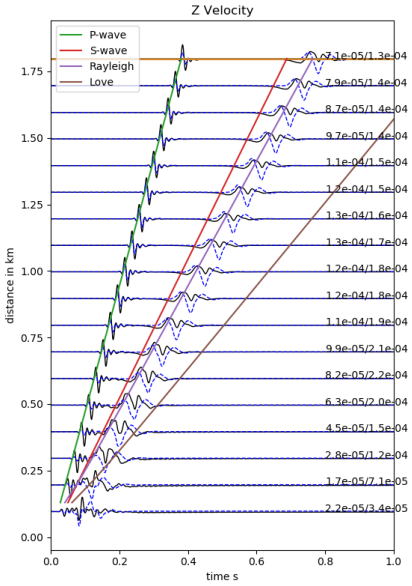
Z Velocity
P-wave
S-wave
Rayleigh
Love
distance in km
time s
7.1e-05/1.3e-04
7.9e-05/1.4e-04
8.7e-05/1.4e-04
9.7e-05/1.4e-04
1.1e-04/1.5e-04
1.2e-04/1.5e-04
1.3e-04/1.6e-04
1.3e-04/1.7e-04
1.2e-04/1.8e-04
1.2e-04/1.8e-04
1.1e-04/1.9e-04
9.9e-05/2.1e-04
8.2e-05/2.2e-04
6.3e-05/2.0e-04
4.5e-05/1.5e-04
2.8e-05/1.2e-04
1.7e-05/7.1e-05
2.2e-05/3.4e-05

(a) (b) (c)

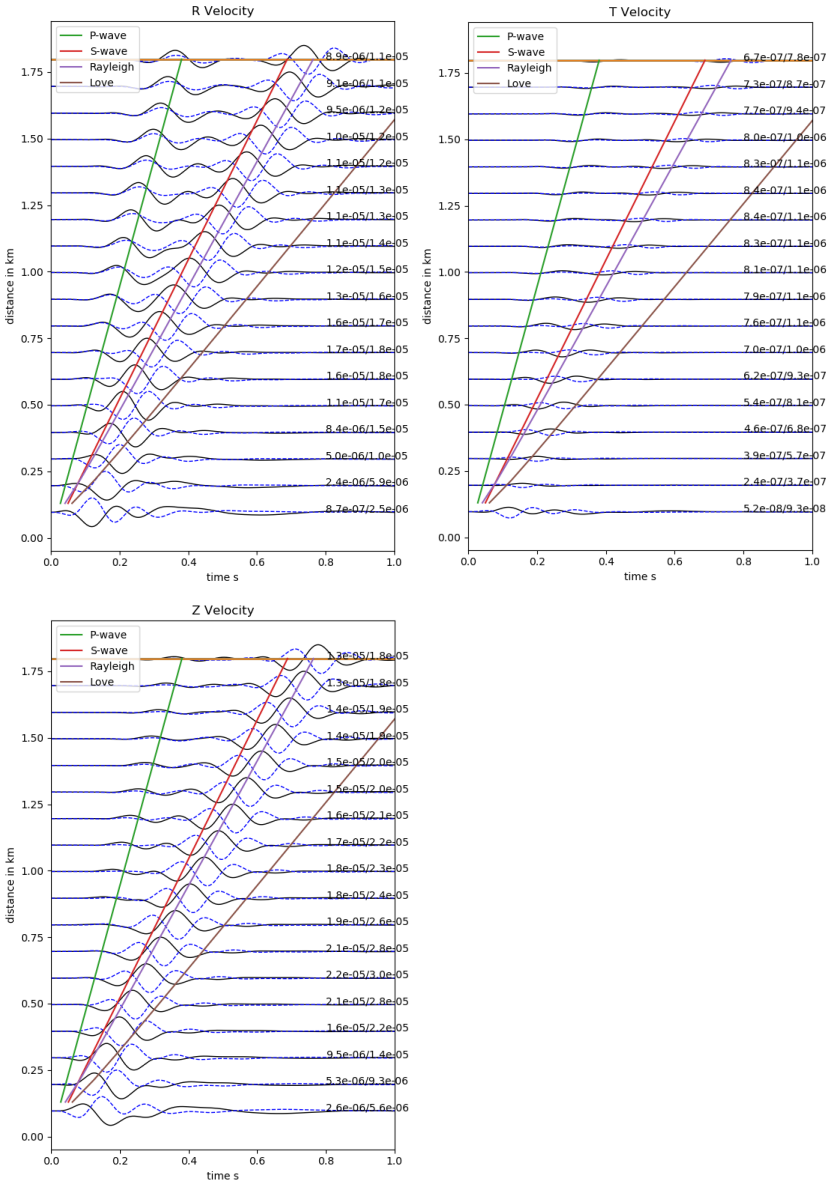

(d) (e) (f)

Figure 15: Distance-time plot of velocity. (a)-(c) 85 Hz filtered (d)-(f) 2-8 Hz filtered.

Since we talked about frequency difference while discussing the velocity result, here we have the spectrum of the data. We can see that the hydrostatic case has much higher amplitude for frequency around 7-20 Hz, which is higher than the frequency of surface wave. But for the RVP wave analysis in fig.17, the two cases have quite similar result, which looks different from the analysis above-mentioned. More verification needs to be done to check the difference.

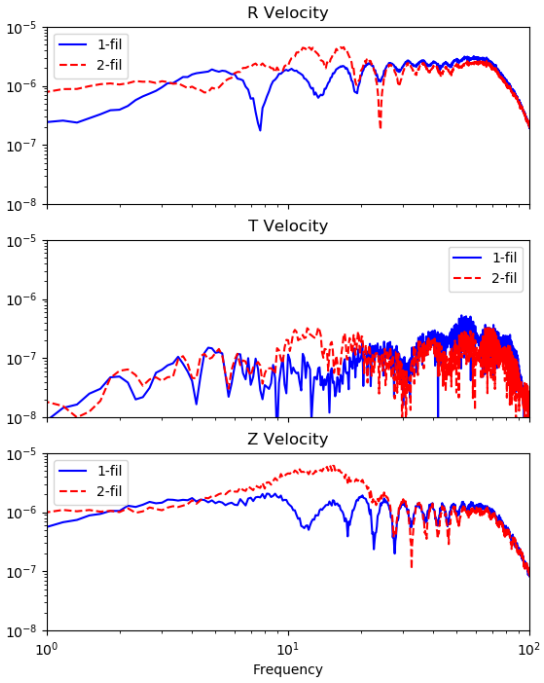

Figure 16: Spectrum of 0.9 km result

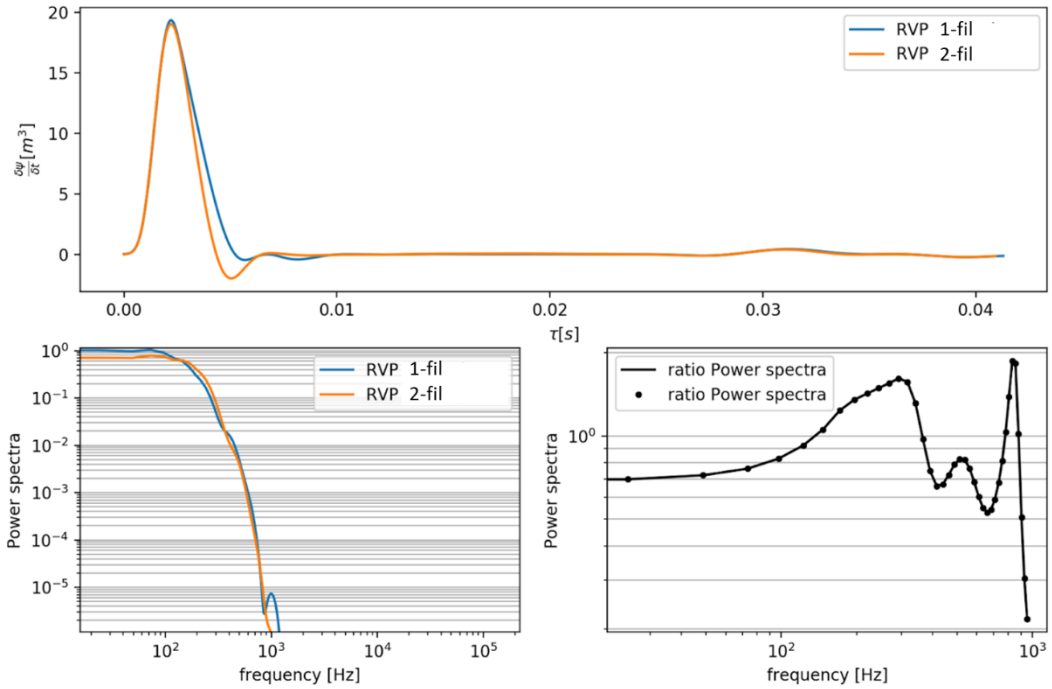

Figure 17: RVP result

Findings

The following findings come from this work:

1. We demonstrate that filtering the times-series prior to using them for driving SPECFEM3D is equivalent to filtering the seismic records generated after the coupling. This result verifies that the whole coupling process implemented in SPECFEM3D is indeed linear. However, we also discovered that the process of filtering including the filtering action itself and any post or pre-processing needed for the operation can introduce some artifacts such as unwanted time-shift and/or change of the low-frequency content.

2. We investigate the role of attenuation by comparing amplitude of waves generated in a model with any attenuation and one with attenuation properties computed using the Olsen et al. (2003) model. Our results show that waves are more and more attenuated with increased distance and for higher wave frequency. These results are consistent with theory and need more quantitative assessment in the future.

3. The displacement time series for the pure SPECFEM3D case at the corner of the coupling box shows some evidence of no cylindrical symmetry.

4. Pure SPECFEM3D case has lower frequency than no-stress-state case.

6. The hydrostatic stress state might affect the vertical displacement, and also the amplitude and frequency of the second wave. The relationship to the RVP analysis needs to be investigated.

Conclusions

The work performed during the summer included numerical modeling of the waveforms generated by the fourth explosion of the SPE series. Different plotting and analysis scripts were put in place to investigate several questions related to the establishment of future end-to-end modeling capabilities. Our findings fail to provide clues to the link between the near-field and far-field so far. More investigation and verification work is needed for this.

Figure	Script file path	Script file name	
2,3	/lustre/scratch4/turquoise/yhlee/deeper_SPE-4P/scripts/Q1	multi_plot_dir_sac.py	

4,5	/lustre/scratch4/turquoise/yhlee/deeper_SPE-4P/scripts/Q2	peak_run1.py	
6	/lustre/scratch4/turquoise/yhlee/deeper_SPE-4P/scripts/Q3	time_series.py	
7	/lustre/scratch4/turquoise/yhlee/deeper_SPE-4P/scripts/Q3	multi_plot_dir_sac.py	
	/lustre/scratch4/turquoise/yhlee/deeper_SPE-4P/scripts/Q3	output.py	to generate differences data
8,9	/lustre/scratch4/turquoise/yhlee/deeper_SPE-4P/scripts/Q3	python multi_plot_dir_diff.py	to plot differences data
10	/lustre/scratch4/turquoise/yhlee/deeper_SPE-4P/scripts/Q3	Plot_Moveout_oneline.py	L1
11	/lustre/scratch4/turquoise/yhlee/deeper_SPE-4P/scripts/Q4	time_series.py	
12	/lustre/scratch4/turquoise/yhlee/deeper_SPE-4P/scripts/Q4	multi_plot_dir_sac.py	
	/lustre/scratch4/turquoise/yhlee/deeper_SPE-4P/scripts/Q4	output.py	to generate differences data
13,14	/lustre/scratch4/turquoise/yhlee/deeper_SPE-4P/scripts/Q4	python multi_plot_dir_diff.py	to plot differences data
15	/lustre/scratch4/turquoise/yhlee/deeper_SPE-4P/scripts/Q4	Plot_Moveout_oneline.py	L1
16	/lustre/scratch4/turquoise/yhlee/deeper_SPE-4P/scripts/Q4	spectrum.py	